Manuscript prepared for Geosci. Model Dev.
with version 5.0 of the LaTeX class copernicus.cls.
Date: 21 April 2014

A simple parameterization of the short-wave aerosol optical properties for surface direct and diffuse irradiances assessment in a numerical weather model

José A. Ruiz-Arias[1,2,3] **and Jimy Dudhia**[3]

[1]Solar Radiation and Atmosphere Modeling Group, Physics Department, University of Jaén, Jaén, Spain
[2]Center of Advanced Studies in Energy and Environment, University of Jaén, Jaén, Spain
[3]Mesoscale and Microscale Meteorology Division, National Center for Atmospheric Research, Boulder, Colorado, USA

Correspondence to: José A. Ruiz-Arias
(jararias@ujaen.es)

Abstract. Broadband short-wave (SW) surface direct and diffuse irradiances are not typically within the set of output variables produced by numerical weather prediction (NWP) models. However, they are being requested frequently by solar energy applications. In order to compute them, a detailed representation of the aerosol optical properties is important. Nonetheless, NWP models typically oversimplify aerosols representation or even neglect their effect. In this work, a flexible method to account for the SW aerosol optical properties in the computation of broadband SW surface direct and diffuse irradiances is presented. It only requires aerosol optical depth at 0.55 μm and the type of predominant aerosol. Other parameters needed to consider spectral aerosol extinction, namely, Angström exponent, aerosol single-scattering albedo and aerosol asymmetry factor, are parameterized. The parameterization has been tested in the RRTMG SW scheme of the Weather Research and Forecasting (WRF) NWP model. However, it can be adapted to any other SW radiative transfer band model. It has been verified against a control experiment using five radiometric stations in the contiguous US. The control experiment consisted of a clear-sky evaluation of the RRTMG solar radiation estimates obtained in WRF when RRTMG is driven with ground-observed aerosol optical properties. Overall, the verification has shown very satisfactory results for both broadband SW surface direct and diffuse irradiances. It has proven effective to significantly reduce the prediction error and constrain the seasonal bias in clear-sky conditions to within the typical observational error in well-maintained radiometers.

1 Introduction

Broadband SW surface total solar irradiance (also known as global horizontal irradiance, GHI) is the sum of broadband SW surface downward direct normal irradiance (DNI, received from the sun's direction) projected onto a horizontal plane and broadband SW surface downward diffuse irradiance (DIF, received from other directions). In general, DIF may also include reflected irradiance from surrounding areas. Direct and diffuse components of GHI are rarely included in predictions made with Numerical Weather Prediction (NWP) models. As GHI is a key component in the representation of energy closure and mass surface fluxes, a better understanding and representation of physical processes may be gained through the use of DNI and DIF fluxes.

In the surroundings of gentle terrain, and provided the atmospheric state is known, GHI can be calculated at reasonable accuracy using simple models that assume isotropic sky and surface conditions. However, in cloudy skies or steep terrain, the isotropy assumption fails. In such a case, a 3D solar radiation model would provide the best GHI predictions (Cahalan et al., 2005; Iwabuchi, 2006; Pincus and Evans, 2009). Nonetheless, these models are so computationally expensive that, in practice, their use is restricted only to concrete applications such as validation studies (Mayer et al., 2010) or the development of simplified parameterizations (Lee et al., 2011). But, if in particular both DNI and DIF are known, the uneven distribution of GHI over complex terrain areas can be determined. Projection of direct irradiance on tilted surfaces is a geometrical problem. The exact computation of diffuse irradiance over the surface would still be unfeasible but, in

practice, isotropic or quasi-isotropic assumptions can be used at reasonable accuracy (Ruiz-Arias et al., 2010, 2011; Manners et al., 2012).

Energy applications are demanding a better modelling of surface solar fluxes. Both GHI and DNI are acquiring greater importance in the energy sector as the rate of built-in solar systems is growing. On the one hand, traditional flat-photovoltaic (PV) systems, the more mature and widely-utilized solar energy technology, are driven primarily by the incoming global irradiance onto the PV plane. As this plane very rarely coincides with the horizontal plane (the common irradiance output in most of the NWP models), a transposition model from the horizontal to the PV plane is inevitable; but accurate transposition models need DNI and DIF irradiances. On the other hand, solar concentrating technologies, both concentrating photovoltaic and solar-thermal plants, are driven primarily by DNI. These technologies increase the overall efficiency of the systems by concentrating DNI using an optical assembly of mirrors. Overall, solar energy systems require long time-series of GHI and DNI fluxes over wide areas for a proper evaluation of the solar potential. But also, very importantly, they require forecasts that enable an improved operation of the plants and maximize the integration rate of solar systems in the power grid without putting the power supply at risk. This is best done with NWP models for forecast horizons from about 4 to 6 hours onward (Diagne et al., 2013; Inman et al., 2013).

Among the downwelling solar fluxes that can be predicted at the surface, most of the NWP models only provide GHI. It is very likely that this has been motivated by the fact that DNI and DIF are challenging to calculate. But, at the same time, also because surface processes affected by solar radiation can be reasonably well represented with GHI alone, as long as the spatial resolution is more than a few km, which has been the typical case so far. Accurate calculation of DIF fluxes is computationally expensive compared with the simple methods that can be used to obtain GHI (e.g., Dudhia, 1989). Also, DNI and DIF are very sensitive to changes in the optically active components of the atmosphere. But the computational capabilities have grown enough to allow the use of more rigorous and precise methods to solve the atmospheric radiative transfer equation. Ruiz-Arias et al. (2013c) provide a comprehensive benchmarking study of some of the short-wave radiation schemes available in the Weather Research and Forecasting (WRF) NWP model and their ability to predict GHI, DNI and DIF under clear-sky conditions in the contiguous US region. Albeit the evaluated models yielded GHI estimates within the observational error range, not all the modelling approaches showed good skills at predicting DNI and DIF. The best results were achieved with the Rapid Radiative Transfer Model for climate and weather models (RRTMG; Iacono et al., 2008). In particular, for the period evaluated, the mean and root-mean square DNI errors when the RRTMG model was run without considering aerosol extinction (default setting in WRF) were 66 $\mathrm{W\,m^{-2}}$(7%) and 72 $\mathrm{W\,m^{-2}}$(8%), respectively (percent magnitudes are relative to the mean observed value). In contrast, when RRTMG was run with instantaneous observations of aerosol optical properties (hereinafter, AOP), the mean and root-mean square errors diminished to 0 $\mathrm{W\,m^{-2}}$(0%) and 9 $\mathrm{W\,m^{-2}}$(1%), respectively. In the case of DIF, the mean and root-mean square errors when the model was not driven by AOP observations were -26 $\mathrm{W\,m^{-2}}$(-34%) and 28 $\mathrm{W\,m^{-2}}$(37%), respectively. When AOP observations were used, the mean and root-mean square errors decreased to 2 $\mathrm{W\,m^{-2}}$(3%) and 5 $\mathrm{W\,m^{-2}}$(6%), respectively.

2 The need for a AOP parameterization

Many NWP models solve, or may solve, the solar radiative transfer in the atmosphere using a two-stream approach, which allows for a fast and approximated solution by assuming azimuthal isotropy in radiant fluxes (Ritter and Geleyn, 1992; Edwards and Slingo, 1996; Chou et al., 1998; Iacono et al., 2008). Radiative transfer solvers in NWP models have been tailored by assuming an infinite and horizontally uniform atmosphere and treating each model column independently. The major practical consequence of the two-stream approximation is a reduction in accuracy at large solar zenith angles. However, it is accurate enough at other conditions for most of the current applications. It allows for a sufficiently detailed description of the solar direct and diffuse fluxes at a low-to-moderate spectral resolution.

In the absence of clouds, aerosols become the dominant driving factor for DNI and DIF fluxes and the greatest source of uncertainty. In particular, the impact of aerosols in DNI is about 3 to 4 times larger than it is in GHI (Gueymard, 2012; Ruiz-Arias et al., 2013a) since an increase (decrease) of aerosol extinction results in a decrease (increase) of DNI and an increase (decrease) of DIF, in the general case. Thus, errors in DNI and DIF fluxes caused by a misrepresentation of the aerosol load partly cancel out in GHI, in the general case. In part, this explains why many NWP models have traditionally neglected the direct impact of aerosol in the assessment of GHI, or why it has been simply accounted for by using climatological values. However, this may result in DNI assessment errors up to 20% (Ruiz-Arias et al., 2013a,c).

Extinction by aerosols is described in radiative transfer problems in terms of three spectral quantities, namely, aerosol optical depth (AOD or τ), single-scattering albedo (SSA or ω_0) and asymmetry factor (ASY or g). Aerosol optical depth is the integral of the extinction coefficient over an atmospheric path. It represents the attenuation by absorption and scattering events through that atmospheric path. Single-scattering albedo is the ratio of the scattering and extinction efficiencies. It represents the relative importance of the scattering events within the total extinction. Finally, asymmetry factor is the first moment of the scattering phase function. It accounts for the preferred direction in which radiation is scat-

tered (Liou, 2002). It is usual to model the spectral variability of AOD using the Ångström law $\tau(\lambda) = \beta\lambda^{-\alpha}$, where λ is the wavelength in μm, β is the AOD measured at λ=1 μm and α is known as Ångström exponent (AE) (Ångström, 1961).

The number and variety of region-wide aerosol datasets has steadily grown in the recent years, from worldwide ground datasets such as the Aerosol Robotic Network (AERONET; Holben et al., 1998) to sensors aboard satellite platforms that regularly sweep the globe, the best well-known being the Moderate-resolution Imaging Spectroradiometer (Remer et al., 2005). Both provide AOP observations that could be used in NWP models to compute DNI and DIF fluxes. Ground observations, essentially from AERONET, provide a reliable and comprehensive AOP description, at a number of wavelengths. However, the spatial coverage is scarce and its near-real-time availability is limited. Thus, in practice, its applicability to NWP model applications is constrained to a reduced number of cases. Satellite retrievals, on the other hand, provide broad spatial coverage but the accuracy of their current estimates is often only reasonable for AOD at 0.55 μm. In recent years, the coupled Atmosphere-Chemistry Numerical Weather Prediction (ACNWP) models have experienced a big advance leveraged by the growing number of available ground and remotely sensed datasets. Now, ACNWP models routinely offer global forecasts of many molecular and particulate components of the atmosphere. Such is the case of the Monitoring Atmospheric Composition and Climate project (MACC, 2013) or the Goddard Earth Observing System model version 5 (GEOS-5, 2013). They compute AOP from prognoses of the chemical composition of the atmosphere and use them to calculate DNI and DIF fluxes. Nonetheless, in general, ACNWP models are computationally expensive and complex to run compared with the regular limited-area NWP models. Also, as they are initialized using mostly satellite observations, they suffer similar biases regarding optical properties of aerosols.

For those applications that are focused on DNI and DIF fluxes, it is convenient to set up a means to use AOP inputs in NWP models from diverse sources. This approach would allow using the best aerosol optical source for each application. In particular, for long-term evaluations of the regional surface solar radiation potential, combined measurements of satellite and/or aerosol transport models and ground sites could be used (Kinne et al., 2013; Ruiz-Arias et al., 2013b). On the other hand, when the application requires forecasts of surface solar radiation, the AOP predicted by global ACNWP models could be used. Nonetheless, since the only accurate aerosol optical parameter typically available is AOD, the rest of the required parameters, namely, SSA, ASY and AE, have to be specified/parameterized based on additional information, when they are not available.

In this work, a parameterization approach for the aerosol optical parameters required by radiative transfer models other than AOD at 0.55 μm is described. In particular, SSA, ASY, and AE are parameterized as a function of built-in reference aerosols and relative humidity. The method is verified in the WRF NWP model using the RRTMG short-wave radiative scheme against a previous experiment in which RRTMG was driven with observed AOD at 0.55 μm, SSA, ASY, AE and precipitable water gathered in the AERONET network. This control experiment is thoroughly described in Ruiz-Arias et al. (2013c). The benefits of the AOP parameterization were evaluated based on the comparison of a one-year WRF simulation against independent surface solar irradiance ground observations in the contiguous US.

Section 3 describes the approach taken for the parameterization of the aerosol optical properties in the RRTMG short-wave radiative transfer model. Sections 4 and 5 present the results of a benchmarking study against a control experiment and the validation against ground observations, respectively. Finally, Section 6 highlights the most important conclusions of this work.

3 The AOP parameterization

The RRTMG SW radiative transfer model solves multiple scattering using a two-stream algorithm (Oreopoulos and Barker, 1999) over 14 spectral bands spanning from 0.2 to 12.2 μm (Table 1). It accounts for extinction by water vapor, carbon dioxide, ozone, methane, oxygen, nitrogen, aerosols, Rayleigh scattering and clouds. In clear skies, the expected accuracy of RRTMG with respect to line-by-line calculations is about 4 $\mathrm{W\,m^{-2}}$ for direct fluxes and about 5 $\mathrm{W\,m^{-2}}$ for diffuse fluxes (Iacono et al., 2008).

Aerosol optical properties, that must be provided to the radiative transfer routine at every grid-cell of the domain being simulated and each spectral band, have been parameterized in terms of the vertically-integrated (total) AOD at 0.55 μm ($\tau_{0.55}$) and built-in reference aerosols, in a similar way as it is done in many detailed radiative transfer models (Ricchiazzi et al., 1998; Gueymard, 2001; Berk et al., 2005; Mayer and Kylling, 2005). The reason to not parameterize AOD is twofold: on the one hand, optical depth is the most determinant property in the solar extinction burden, so it is important to make use of the best estimate available. On the other hand, unlike other aerosol optical properties, both satellite retrievals and ACNWP models provide reasonable estimates of AOD for many current applications. The reason to choose the value at 0.55 μm is to be consistent with the values usually provided by these data sources and the ground observations at AERONET. Observed AOD can be easily interpolated to a wavelength of 0.55 μm from other spectral values by using the Ångström law. The built-in reference aerosols are used to provide spectral values for SSA, ASY and AE, which are afterwards modulated in terms of the relative humidity to account for the aerosol hygroscopicity.

Two different reference aerosols from Shettle and Fenn (1979), namely rural and urban, have been included so far in WRF. They are representative of broad continental climate

Table 1. Spectral bands distribution in RRTMG. From top to bottom rows, λ's (in nm) are band mean, band minimum and band maximum values, respectively. Note the band numbering does not follow increasing or decreasing wavelength values. The band naming convention follows the RRTMG's definition.

Band #	1	2	3	4	5	6	7	8	9	10	11	12	13	14
$\bar{\lambda}$	3462	2789	2325	2046	1784	1463	1271	1010.1	701.6	533.2	393.1	304.0	231.6	8021
λ_{min}	3077	2500	2150	1942	1626	1299	1242	778.2	625.0	441.5	344.8	263.2	200.0	3846
λ_{max}	3846	3077	2500	2150	1942	1626	1299	1242.0	778.2	625.0	441.5	344.8	263.2	12195

conditions. The rural aerosol is intended for situations where the aerosol is not expected to be affected by urban or industrial sources. Thus, it is expected to be the typical choice for most of the simulations. It is composed of a mixture of 70 percent of water soluble substance and 30 percent dust-like aerosols. The urban aerosol is a mixture of rural aerosol (80 percent) and soot-like particles (20 percent). The two reference mixtures define the absorption, scattering and extinction coefficients, single-scattering albedo and asymmetry parameter for a number of wavelengths and relative humidities from 0% to 99%. The choice of these two reference aerosols has been based on the fact that they have demonstrated their ability to represent reasonably well clear-sky surface solar fluxes in other radiative transfer models (Ricchiazzi et al., 1998; Gueymard, 2001, 2008).

3.1 Aerosol optical depth and Ångström exponent

Aerosol optical depth has to be specified at each RRTMG spectral band. In real applications, even in the best cases, AOD is only known/measured at a small number of wavelengths, and the Ångström law is often used to describe its spectral variability. But, for some aerosol particle ensembles, such as the reference aerosol mixtures used here, this spectral variability is best described using a 2-band version of the Ångström law (Gueymard, 2001) as follows:

$$\tau(\lambda) = \tau_{0.55} \left(\frac{\lambda}{0.55} \right)^{-\alpha_i}, \quad (1)$$

where λ is the wavelength in $\mu\mathrm{m}$ and α_i is the Ångström exponent for each band, defined as $\alpha_i = \alpha_1$, for $\lambda <$0.55 $\mu\mathrm{m}$, and $\alpha_i = \alpha_2$, otherwise. The coefficients α_i are obtained from the built-in reference aerosols by linearly fitting (in log-log coordinates) the spectral extinction coefficients tabulated in Shettle and Fenn (1979) for each aerosol mixture and relative humidity. The corresponding values of α_i are given in Table 2. For α_1, the extinction coefficients at 0.337 $\mu\mathrm{m}$, 0.55 $\mu\mathrm{m}$ and 0.649 $\mu\mathrm{m}$ were used. The values at 0.649 $\mu\mathrm{m}$, 1.06 $\mu\mathrm{m}$ and 1.536 $\mu\mathrm{m}$ were used for α_2. This modelling approach resolves better than the regular Ångström law the distinct spectral contribution of the fine and coarse modes of the aerosol size distribution. The fact that α_1 and α_2 show distinct values suggests this approach is pertinent. The limit for the calculation of α_1 and α_2 (λ=0.55 $\mu\mathrm{m}$) is similar to the limit of 0.6 $\mu\mathrm{m}$ suggested by Dubovik et al. (2002) to distinguish between the fine mode and the coarse mode in bimodal size distributions. The decreasing α_i values for increasing relative humidities indicate a particle size increase by water uptake and a shift of the extinction towards lower wavelengths. It is worth mentioning that, unlike expected, Ångström exponents for the rural aerosol are greater than for the urban aerosol, indicating that overall the particles in the urban mixture have a larger size. This is very likely due to the assumption made in Shettle and Fenn (1979) that the soot-like particles in the urban mixture have the same size distribution than the water soluble and dust-like particles in the rural aerosol mixture despite the fact that soot particles are in general of smaller size.

Aerosol optical depth was averaged over each spectral band in order to provide a representative value over that entire band. As the solar spectral irradiance changes abruptly in the ultraviolet and visible regions and some model bands in the infrared region are wide, the extraterrestrial solar spectrum, $E_{0n}(\lambda)$, as described by Gueymard (2004), was used as a weighting factor to compute the average AOD value, $\bar{\tau}_{rj}$, as follows:

$$\bar{\tau}_{rj} = \frac{\int_{\Delta\lambda_j} E_{0n}(\lambda)\tau_r(\alpha_{ri};\lambda)d\lambda}{\int_{\Delta\lambda_j} E_{0n}(\lambda)d\lambda}, \quad (2)$$

where j stands for each RRTMG spectral band, that extends over the range $\Delta\lambda_j$, and $\tau_r(\alpha_{ri};\lambda)$ is the aerosol optical depth calculated with Eq. (1) for the relative humidity r. Factorizing $\tau_{0.55}$ out of $\tau_r(\alpha_{ri};\lambda)$, Eq. (2) can be re-written as

$$\bar{\tau}_{rj} = \rho_{rj}\, \tau_{0.55} \quad (3)$$

where ρ_{rj} is the spectral scale factor with respect to $\tau_{0.55}$ for the band j and relative humidity r. It is given by

$$\rho_{rj} = \frac{\int_{\Delta\lambda_j} E_{0n}(\lambda) \left(\frac{\lambda}{0.55} \right)^{-\alpha_{ri}} d\lambda}{\int_{\Delta\lambda_j} E_{0n}(\lambda)d\lambda}. \quad (4)$$

Equation (4) was numerically evaluated for each spectral band and relative humidity according to the α_i coefficients in Table 2. The so-computed spectral scale factor values ρ_{rj} were grouped in two look-up-tables (LUT) for the two

Table 2. Ångström exponents for each band, aerosol mixture and relative humidity.Ångström exponents were computed as described in Sect. 3.1

Relative humidity	α_i	0%	50%	70%	80%	90%	95%	98%	99%
Rural	α_1	1.036	1.035	1.030	0.999	0.946	0.906	0.818	0.753
	α_2	1.433	1.430	1.421	1.382	1.371	1.357	1.221	1.152
Urban	α_1	0.915	0.919	0.929	0.921	0.875	0.803	0.682	0.588
	α_2	1.198	1.202	1.202	1.254	1.265	1.243	1.164	1.082

aerosol types (Tables A1 and A2). For each RRTMG spectral band, the spectral scaling factors are interpolated using a 4-points Lagrange interpolation at the relative humidity values predicted by the NWP model. Aerosol optical depth is then calculated using Eq. (3) and the input $\tau_{0.55}$. Figure 1 illustrates the interpolation results for the rural aerosol mixture. It also compares the E_{0n}-weighted average as defined by Eq. (2) with a regular (un-weighted) average. The largest discrepancies appear in the ultraviolet, visible and near-infrared regions (bands 8-12) as well as in the mid-infrared region (band 14). The weighted average shifts the averaged AOD value towards wavelengths with higher extraterrestrial solar intensity resulting in an enhancement of aerosol extinction in the visible and infrared bands, and a decreased extinction in the ultraviolet region.

3.2 Single-scattering albedo and asymmetry factor

Shettle and Fenn (1979) provides spectral values of SSA and ASY up to 40 μm starting at 0.2 μm for each aerosol mixture and relative humidity value. Single-scattering albedo has been spectrally weighted for each band as follows:

$$\bar{\omega}_{o,rj} = \frac{\int_{\Delta\lambda_j} E_{on}(\lambda)\hat{\omega}_{o,r}(\lambda)\tau_r(\alpha_{ri};\lambda)d\lambda}{\int_{\Delta\lambda_j} \tau_r(\alpha_{ri};\lambda)E_{on}(\lambda)d\lambda}, \quad (5)$$

where $\bar{\omega}_{o,rj}$ is the average SSA value for the relative humidity r and the spectral band j. The tabulated values of SSA for each relative humidity were interpolated using cubic splines to the wavelengths at which $E_{on}(\lambda)$ is known, resulting in the values $\hat{\omega}_{o,r}(\lambda)$. Equation (5) assigns a higher weight to the wavelengths at which extraterrestrial solar spectral irradiance and aerosol extinction are greater. The values $\bar{\omega}_{o,rj}$ were grouped in two LUTs for the two aerosol mixtures (Tables A3 and A4) from which values are interpolated for each spectral band and relative humidity using a 4-points Lagrange interpolation.

Following a similar approach, spectrally-averaged asymmetry factor has been calculated as:

$$\bar{g}_{rj} = \frac{\int_{\Delta\lambda_j} E_{on}(\lambda)\hat{g}_r(\lambda)\hat{\omega}_{o,r}(\lambda)\tau_r(\alpha_{ri};\lambda)d\lambda}{\int_{\Delta\lambda_j} \hat{\omega}_{o,r}(\lambda)\tau_r(\alpha_{ri};\lambda)E_{on}(\lambda)d\lambda}, \quad (6)$$

where $\bar{g}_{rj}$ is the average ASY value for the relative humidity r and the spectral band j. The tabulated values of ASY for each relative humidity were interpolated using cubic splines to the wavelengths at which $E_{on}(\lambda)$ is known, resulting in the values $\hat{g}_r(\lambda)$. In this case, a higher weight has been assigned at those wavelengths with greater $E_{on}(\lambda)$ and scattering coefficient. The values $\bar{g}_{rj}$ were grouped in two look-up-tables for the two aerosol types (Tables A5 and A6) from which values are interpolated for each spectral band and relative humidity using a 4-points Lagrange interpolation.

Figure 2 shows the parameterized SSA and ASY values for the two built-in reference aerosols for a relative humidity of 80%. The solid thin line is the resulting interpolation from the tabulated values (cross marks) in Shettle and Fenn (1979), both for SSA and ASY. The solid thick line is the resultant E_{0n}-weighted average for each model band after applying Eqs. (5 and 6). The shaded region represents the range of variability at each band due to relative humidity, from 0% to 99%. In general, SSA for the urban aerosol (Fig. 2c) has a smaller value at all wavelengths and a higher sensitiviy to relative humidity changes than the rural (Fig. 2a). Thus, the latter scatters more radiation but responds less to changes in humidity. Note that, for wavelengths above 4 μm, the band-averaged SSA keeps close to the SSA value between 4 and 5 μm because the extraterrestrial solar intensity is very small beyond 5 μm. The comparison with SSA values observed at AERONET reveals that the urban SSA takes abnormally low values with respect to average conditions. This fact suggests that the rural aerosol should be preferred. However, it is still appropriate to maintain the urban aerosol since there might be particular cases, normally short in time or limited in area, where it is required to assume a high aerosol absorptance.

The asymmetry factor values are very similar for the two built-in aerosol mixtures (Figs. 2b and 2d), with decreasing forward scattering in the ultraviolet and visible bands and increasing in the infrared up to 3 μm. Beyond, it stays at about 0.75.

3.3 Vertical distribution

The vertical distribution of AOD is modelled after the spectral disaggregation has been completed. The latter is made following Eq. (3) with spectral scale values ρ_{rj} interpolated according to the model relative humidity, but only at the surface level. Then, the spectrally disaggregated $\bar{\tau}_j$ values at the

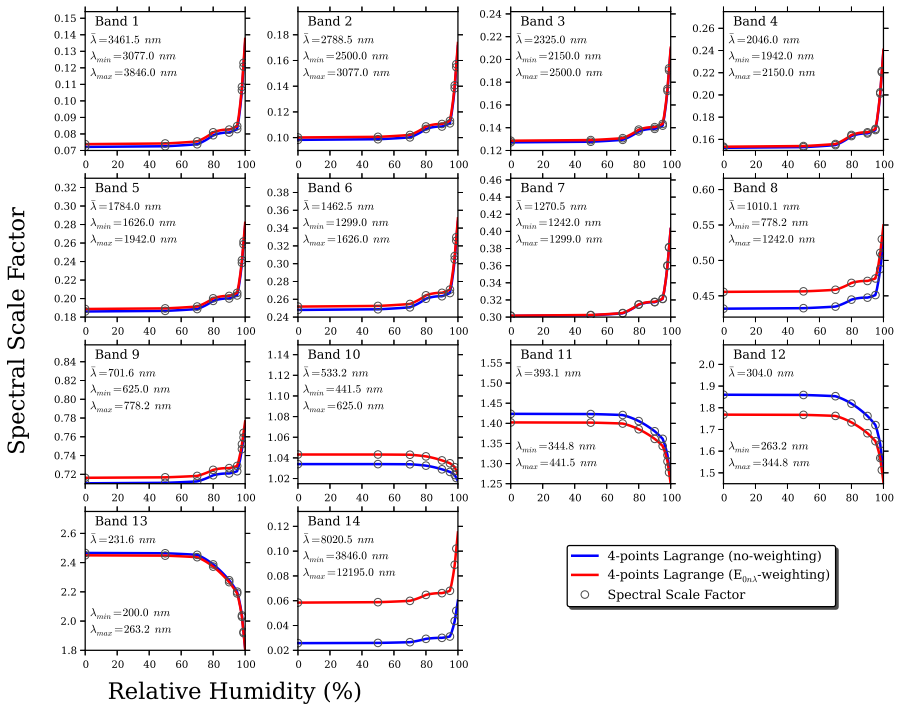

Fig. 1. AOD spectral scale factor interpolated using 4-point Lagrange interpolation for relative humidities from 0% to 99% for each RRTMG spectral band and the rural aerosol. For the sake of comparison, the results using weighted and un-weighted spectral scale factors are shown.

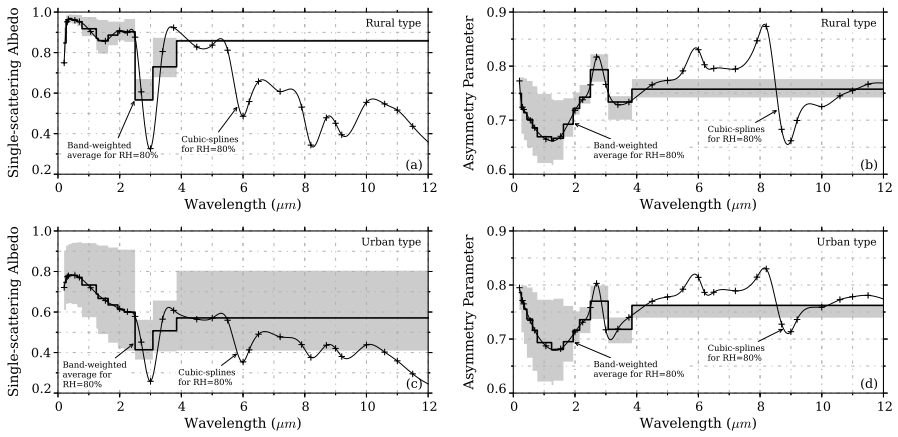

Fig. 2. Parameterized SSA and ASY parameters for the rural and urban aerosol mixtures for a relative humidity of 80% (thick line). The Shettle and Fenn (1979) spectral values are shown with cross marks. They have been interpolated using cubic splines (thin line). The grey region encompasses the variability range of the parameters with different values of relative humidity.

surface for each band are distributed in the vertical according to an exponential profile (Ruiz-Arias et al., 2013c) as follows:

$$\bar{\tau}_j(z) = \frac{\bar{\tau}_j / Z_h}{e^{-\frac{z_{sfc}}{Z_h}} - e^{-\frac{z_{toa}}{Z_h}}} \int_z^{z_{toa}} e^{-\frac{z}{Z_h}} dz, \tag{7}$$

where z_{sfc} and z_{toa} are the altitudes at the surface and the top of the atmosphere, respectively. The height scale parameter Z_h is set to 2.5 km (Gueymard and Thevenard, 2009). By following this procedure the vertically-integrated profile of AOD is consistent with the $\tau_{0.55}$ value provided as input.

The vertical distribution of SSA and ASY is based only on the relative humidity profile in the NWP model. Therefore, the SSA and ASY vertical profiles resemble the model moisture profile.

4 Parameterization benchmarking

The consistency of the AOP parameterization at predicting clear-sky surface solar irradiance has been first benchmarked against a case study (hereinafter referred to as control experiment) in which the WRF's RRTMG model was driven using observed aerosol optical properties and precipitable water values at a number of the AERONET network sites with collocated surface solar irradiance observations. The control experiment represents a best-case estimate of the expected model performance at predicting clear-sky surface solar irradiance.

4.1 Control experiment

In the control experiment, the WRF model was run using the RRTMG SW scheme. Clear-sky estimates of GHI, DNI and DIF were computed every 10 minutes for five completely cloudless days at five different locations in the contiguous US (see Ruiz-Arias et al. (2013c) for a description of the sites). At all sites, concurrent observations of GHI, DNI and DIF, as well as aerosol optical properties and precipitable water from nearby AERONET locations, were available. Four of the experimental surface solar irradiance sites belong to the Baseline Surface Radiation Network (BSRN; Ohmura et al., 1998) and the Surface Radiation Network (SURFRAD; Augustine et al., 2005). The fifth is at the Atmospheric Radiation Measurement (ARM) Central Facility, in Oklahoma, USA. The WRF model was modified such that instantaneous observations of the aerosol optical properties and precipitable water at the AERONET sites were ingested every 10 minutes at exactly the same time steps at which solar irradiance was computed in the model. The few traces of clouds generated by WRF during the simulations were cleared up by setting the cloud mixing ratio to zero in order to ensure completely clear-sky conditions. Note that, as all the aerosol optical properties were ingested from ground observations, there was no need to parameterize any aerosol property. Thus, the control experiment gives a fair estimate of the RRTMG model performance at computing clear-sky GHI, DNI and DIF. The control experiment is fully described in Ruiz-Arias et al. (2013c).

4.2 Test case

The simulations of the control experiment were repeated using the AOP parameterization. That is, only the observed AOD at 0.55 $\mu\mathrm{m}$ at the AERONET sites and the type of aerosol were provided to WRF. The rest of the aerosol parameters, namely, AE, SSA and ASY, were parameterized, as presented in Sect. 3. As in the control experiment, the model was driven with observations of precipitable water so that the real skill of the aerosol parameterization was better evaluated. Two different simulations, assuming rural and urban aerosols, were carried out at each site. Note however that the urban aerosol is so absorbing that it should not be adequate for most of the real conditions. An additional simulation for a completely clean atmosphere (i.e., zero aerosols) was also conducted.

Figure 3 shows the relative errors of both the control experiment and the test cases as compared against the GHI, DNI and DIF ground observations at each site and the composite of all sites (referred to as case ALL in Fig. 3). If the parameterization were perfect, the grey blocks and the colour bars should match. Disagreements are caused by the prescription of the aerosol optical properties.

Figure 3a shows the relative errors in the case of DNI. As expected, the discrepancies between the control experiment and the test cases using the AOP parameterization are negligible (below 1% at all sites), regardless the choice of aerosol mixture. The reason is that, as far as aerosols are concerned, DNI is only impacted by optical depth, and the AOD at 0.55 $\mu\mathrm{m}$ is the same in both the control experiment and the test cases. The only distinction between the experiments is the AOD spectral distribution, modelled by the AE value. In the control experiment, it comes from spectral observations of AOD. However, in the test cases, it is inferred from the selected reference aerosol and the relative humidity. Nonetheless, as DNI is a broadband quantity, the impact of AE is reduced and so are the differences between the control experiment and the test cases. On the contrary, when aerosols impact is not considered, the simulated DNI overestimates the observations beyond the expected observational error.

Figure 3b shows the relative errors in the case of DIF. Discrepancies between the control experiment and the test cases are greater than for DNI because DIF is also impacted by SSA and ASY, which now are parameterized. Specifically, for relative humidities below 90%, the urban aerosol is about 20% to 40% more absorbing than the rural aerosol. As a consequence, systematic disagreements up to 15-20% appear in the DIF values computed with the two aerosol mixtures. Hence, unlike for the DNI, the choice of the correct aerosol is important for DIF. In particular, at four of the sites evaluated in this study, the rural aerosol fits reasonably well the control experiment. At the TBL site, however, the urban aerosol yielded better results because the particular selection of clear-sky days for this site showed an anomalously high rate of absorbing aerosols that might be explained by

the presence of wildfires nearby in the Arapaho-Roosevelt National Forest, at 50 to 100 km away from the validation sites (Short, 2013; Ruiz-Arias et al., 2013c). This case serves nonetheless to show that the urban mixture is useful in some circumstances. When the aerosols impact is not considered, a systematic underestimation around 30% appears.

In the case of GHI (Fig. 3c), all the experiments provide estimates within the expected observational error range, even when aerosols are not provided because, as already commented, the large overestimation in DNI is partly cancelled out with the large underestimation in DIF. Overall, the rural aerosol fits better the control experiment.

5 Validation against ground observations

A major limitation of the benchmarking study described in the former section comes from the fact that AOD, AE, SSA and ASY need to be all known simultaneously. Measurement of SSA and ASY is limited by strong practical constraints (Dubovik et al., 2000) that reduce drastically their availability. Nonetheless, since the only external input required by the AOP parameterization is AOD at 0.55 μm, the validation period with the AOP parameterization can be extended as long as AOD and surface solar irradiance measurements are available. Thereby, two one-year-length simulations have been conducted using the AOP parameterization with rural and urban aerosols at the same five sites described in Sect. 4 and with the same model set-up. In particular, the AOD at 0.55 μm from the AERONET sites was ingested into WRF every 10 minutes at exactly the same time steps at which GHI, DNI and DIF were computed. The subsequent validation was conducted only for those time steps with AOD observations under clear-sky conditions, which were discerned based on the method described in Long and Ackerman (2000).

In addition, the simulation was repeated using the WRF's Dudhia SW scheme as a skill reference for the case of GHI. The Dudhia SW scheme is the radiative transfer model of choice in most of the WRF runs. It is a simple broadband parameterization (one single spectral band) that considers extinction by Rayleigh atmosphere and water vapor. It does not account for multiple scattering effects. Extinction by ozone, aerosols, and other molecular absorbers is not explicitly parameterized (Dudhia, 1989). Instead they are all accounted for by using a bulk scattering parameter that was empirically fixed for average turbidity conditions (Zamora et al., 2003, 2005). Further references may be found in Ruiz-Arias et al. (2013c).

5.1 Dynamical range performance

The performance of the AOP parameterization for each aerosol type has been analysed throughout the entire range of the aerosol optical properties observed in the five experimental sites. Figure 4(a-c) shows the relative frequency distribution of the observed AOD at 0.55 μm, the observed and parameterized SSA values, and the observed and parameterized ASY values, respectively. Overall, the AOD values observed in the validation sites are small, although the evaluation period spans an entire year and includes all the available observations at the validation sites. The mean value is 0.06, the median is at 0.05 and 95% of the values are smaller than 0.12. The mean observed SSA value is 0.92, with 95% of the values greater than 0.75. A very distinct estimation of the SSA values is made with the rural and urban mixtures. For the rural aerosol, 95% of the SSA values are between 0.92 and 0.94, with a mean value of 0.93. For the urban aerosol, 95% of the SSA values are smaller than 0.68, and the mean value is 0.62. Figure 4c shows the relative frequency distribution of observed and simulated ASY values. Ninety-five percent of the observations span the range from 0.61 to 0.75, with a mean value of 0.67. The values simulated by the rural aerosol have a mean of 0.66, and 90% of the data spans from 0.63 to 0.67. In the case of the urban aerosol, 90% of the aerosols span from 0.66 to less than 0.67, and the mean is also 0.66.

As AE is not directly parameterized (note that it has been approximated by means of a two-band model), it has not been shown for the sake of simplicity. However, its effective value can be estimated from the spectral distribution of AOD throughout the RRTMG bands. When that is done, 99% of the AE values for the rural aerosol are between 1.19 and 1.22, and 99% of the AE values for the urban aerosol are in the range from 1.00 to 1.06. In contrast, 90% of the observations go from 0.72 up to 2.59. Note thus that, the effective AE values used in the parameterization do not span the range of observed AE values.

Figure 4d-f shows the results for DNI. In each case, the relative error is within the expected DNI observational error. However, as it can be seen in Fig. 4d, for AOD above 0.05, there is a systematic bias of about 4 Wm^{-2} between the estimates with the rural and urban aerosol mixtures. An experiment (not shown here for the sake of conciseness) conducted with the SMARTS radiative transfer model (Gueymard, 2001) has revealed this discrepancy is compatible with the different AE values modeled by each aerosol type. For AOD values below 0.05, the disagreement with the observations increases slightly. As shown in Ruiz-Arias et al. (2013c), this might be related to the observational uncertainty of the AOD observations taken at AERONET sites. As expected, DNI does not show any apparent trend with SSA and ASY (Fig. 4e-f).

Figure 4g-i shows the results for DIF. For these sites, and for all cases, the DIF estimates for the rural aerosol are within the expected range of the observational error. However, the urban aerosol shows a negative bias that, in particular, increases in magnitude for increasing AOD. The reason is that there exists a positive correlation between AOD and SSA in this experimental dataset (not shown here) such as an in-

crease of AOD entails an increase of SSA. In addition, as shown in Fig. 4h, there exists a systematic underestimation of about 15% in the estimated DIF values assuming the urban aerosol, whereas it stays unbiased for the rural aerosol. No trend is observed in the simulated DIF values with respect to ASY (Fig. 4i).

Figure 4j-l shows the results for GHI. Besides GHI computed with the RRTMG model assuming rural and urban aerosols, GHI calculated with the Dudhia SW scheme is also shown. It does not make use of any aerosol optical variable as input. In any case, all the simulated values are within the range of the expected observational error. In particular, GHI estimates with the RRTMG model assuming rural aerosol are always unbiased. On the contrary, when the urban aerosol is assumed, the bias in DIF (Fig. 4g-i) appears in GHI but with a reduced relative impact (about 3%). The Dudhia scheme shows an increasing trend with respect to AOD at 0.55 μm that goes from an underestimation of about 5% (or, equivalently, 25 Wm^{-2}) for very clean conditions to unbiased estimates for AOD about 0.12, as expected for a scheme with a fixed aerosol scattering parameter. No trend is observed with respect to SSA and ASY.

5.2 Seasonality

One of the particular benefits of having a method to include aerosol extinction in the computation of surface solar irradiance is to consider the impact of the seasonal variability of AOD in surface fluxes. Specifically, if AOD is not considered in the calculation of clear-sky surface irradiance, or it is done using a fixed value, a seasonal bias may appear in the computed irradiances at the surface, which can become considerably large depending on the simulated region. Figure 5 shows the daily mean relative error in computed DNI, DIF and GHI (simulated values minus observations, relative to the observations) using the RRTMG model assuming rural and urban aerosols, throughout the simulated year over the composite of the five experimental sites. A 15-day moving average filter has been used to make clear the bias trend. For GHI, the calculated values with the Dudhia scheme are also shown. The expected observational error region for the surface solar irradiance observations, roughly estimated as $\pm 5\%$, is highlighted in yellow.

Figure 5a and b shows the case of DNI and DIF estimates, respectively. Overall, both the rural and urban aerosol mixtures produce unbiased DNI values during the entire simulated year. The little disagreement between them is due to the different AE values that are parameterized by each aerosol mixture. Regarding DIF, the urban aerosol yields a sustained bias around -15%, with no seasonal trend, whereas the bias using the rural aerosol stays within the expected observational error region, also without clear seasonal trend. Note that it proves the rural aerosol fits the observations better for the evaluated sites.

Figure 5c shows the results for GHI. The values computed with the RRTMG model for the rural aerosol are unbiased throughout the entire simulated year, whereas the assumption of urban aerosol introduces a negative bias about -2%. But no seasonal trend is observed in either of these two cases. On the contrary, the Dudhia model shows a clear seasonal trend in the bias, which underestimates by up to 5% in winter, since it includes an empirically fixed atmospheric scattering in a yearly basis. Thus, it considers so much scattering in winter, and so little in summer than it cannot reproduce the GHI intra-annual variability.

6 Discussion and conclusions

A parameterization of the aerosol optical properties for short-wave surface solar irradiance assessment, including direct and diffuse components, in NWP models has been proposed. It has been implemented and verified in the RRTMG SW scheme of the WRF NWP model. The verification has been conducted in five radiometric stations with nearby or collocated AERONET sites in the contiguous US and also relies on a previous experiment that has been used here as control case. The control experiment consisted of a best-case clear-sky evaluation of some of the WRF short-wave solar radiation schemes forced with observed aerosol optical properties taken at the AERONET sites. Thus no aerosol optical property is parameterized in the control experiment. On the contrary, the aerosol optical parameterization only uses observations of AOD at 0.55 μm, and AE, SSA and ASY are parameterized based on the predominant type of aerosol and the relative humidity.

The approach to parameterize the aerosol optical properties is versatile since the only mandatory parameter is AOD at 0.55 μm, which can be provided either as a fixed value or as a time and space varying field. The rest of aerosol optical parameters, namely, AE, SSA and ASY are parameterized from a choice between two bimodal aerosol mixtures, namely rural and urban, dominated by the accumulation mode, the urban being a more absorbing version of the rural aerosol. However, as for AOD at 0.55 μm, AE, SSA and ASY can also be provided either as a fixed value or as a time and space varying field. This allows for sensitivity studies or the use of external data sources. The aerosol parameterization based on the aerosol mixture choice allowed us to extend the evaluation period up to one year, beyond the comparison with the control case. Overall, the verification has shown very satisfactory results. Regardless of the reference aerosol that is invoked, DNI using the AOP parameterization is almost identical to the control case. The very small mismatches shown result from the parameterization of AE. When the focus is on DIF, the selection of the right reference aerosol is important because DIF is affected also by SSA and ASY. In four of the experimental sites, the rural aerosol resulted in very good agreement with the control case. In the remaining

site, the SSA values registered in the AERONET station were anomalously low. This explains why the urban aerosol was better and proves that its use can be effective to consider the effect of high absorbing aerosols. Based on the 1-year simulation, it has been proved that the use of the AOP parameterization to consider time-varying aerosols contributes to effectively removing seasonal biases in DNI, DIF and GHI. In the latter case, this has been illustrated by comparing the results against the Dudhia short-wave scheme, which considers aerosol extinction by assuming a single yearly value.

Arguably, a major limitation of the AOP parameterization might be the requirement to adhere to one of the prescribed aerosol mixtures. But this method still makes sense for limited-area models under the assumption that significant changes regarding the aerosol type occur at spatial scales larger than the domain being simulated with WRF.

The included aerosol mixtures do not allow simulating aerosol situations with dominant coarse mode such as those for sea salt or desert dust. The inclusion of such an aerosol mixture is an on-going task that will allow us to extend the validation areas to regions with higher AOD. The task has being initiated by evaluating the RRTMG model in arid sites, which are usually subjected to high turbidities. This preliminary study will allow isolating the radiative transfer errors from the aerosol model errors. Finally, it is worth mentioning that the modelling of aerosol extinction for the computation of GHI, DNI and DIF based on built-in aerosol mixtures, as here presented, is an approach to this problem. An alternative approach indicated at larger scales is the use of a climatology of the aerosol optical properties.

Appendix A

Look-up-tables

In this section we present the look-up-tables used in the parameterization of the AOD spectral scaling factor, single-scattering albedo and asymmetry parameter for the rural and urban reference aerosols.

A1 AOD spectral scale factor

A2 Single-scattering albedo

A3 Asymmetry parameter

Acknowledgements. The authors would like to thank the BSRN, NOAA, and AERONET science teams, and the ARM Climate Research Facility, for establishing and maintaining the sites used in this investigation. The authors also warmly thank Christian A. Gueymard for his unbounded support and stimulating discussions in the course of this research. José A. Ruiz-Arias is funded by a Marie Curie Action under the project PIOF-GA-2010-273648 within the 7th European Community Framework Programme, the Spanish Ministry of Science and Innovation under the project CGL2011-30377-C02-01 and FEDER funds through the Junta de Andalucia research group TEP-220. This work was carried out while the author was hosted by NCAR.

References

Ångström, A.: Techniques of determinig the turbidity of the atmosphere 1, Tellus, 13, 214–223, 1961.

ARM: http://www.arm.gov/sites/sgp/c, Last accessed: 7 November 2013.

Augustine, J. A., Hodges, G. B., Cornwall, C. R., Michalsky, J. J., and Medina, C. I.: An update on SURFRAD–The GCOS Surface Radiation budget network for the continental United States, J. Atmos. Ocean. Technol., 22, 1460–1472, 2005.

Berk, A., Anderson, G. P., Acharya, P. K., Bernstein, L. S., Muratov, L., Lee, J., Fox, M. J., Adler-Golden, S. M., Chetwynd, J. H., Hoke, M. L., Lockwood, R. B., Cooley, T. W., and Gardner, J. A.: MODTRAN5: A reformulated atmospheric band model with auxiliary species and practical multiple scattering options, 2005.

Cahalan, R. F., Oreopoulos, L., Marshak, A., Evans, K. F., Davis, A. B., Pincus, R., Yetzer, K. H., Mayer, B., Davies, R., Ackerman, T. P., Barker, H. W., Clothiaux, Eugene Eand Ellingson, R. G., Garay, M. J., Kassianov, E., Kinne, S., Macke, A., O'Hirok, W., Partain, P. T., Prigarin, S. M., Rublev, A. N., Stephens, G. L., Szczap, F., Takara, E. E., Várnai, T., Wen, G., and Zhuravleva, T. B.: THE I3RC: Bringing together the most advanced radiative transfer tools for cloudy atmospheres, Bull. Am. Meteorol. Soc., 86, 1275–1293, 2005.

Chou, M.-D., Suarez, M. J., Ho, C.-H., Yan, M. M., and Lee, K.-T.: Parameterizations for cloud overlapping and shortwave single-scattering properties for use in general circulation and cloud ensemble models, J. Clim., 11, 202–214, 1998.

Diagne, M., David, M., Lauret, P., Boland, J., and Schmutz, N.: Review of solar irradiance forecasting methods and a proposition for small-scale insular grids, Renew. Sust. Energy Rev., 27, 65–76, 2013.

Dubovik, O., Smirnov, A., Holben, B., King, M., Kaufman, Y., Eck, T., and Slutsker, I.: Accuracy assessments of aerosol optical properties retrieved from Aerosol Robotic Network (AERONET) Sun and sky radiance measurements, J. Geophys. Res. Atmos., 105, 9791–9806, 2000.

Dubovik, O., Holben, B., Eck, T. F., Smirnov, A., Kaufman, Y. J., King, M. D., Tanré, D., and Slutsker, I.: Variability of absorption and optical properties of key aerosol types observed in worldwide locations, J. Atmos. Sci., 59, 2002.

Dudhia, J.: Numerical study of convection observed during the winter monsoon experiment using a mesoscale two-dimensional model, J. Atmos. Sci., 46, 3077–3107, 1989.

Edwards, J. and Slingo, A.: Studies with a flexible new radiation code. I: Choosing a configuration for a large-scale model, Q. J. R. Meteorol. Soc., 122, 689–719, 1996.

GEOS-5: http://http://gmao.gsfc.nasa.gov/GEOS/, Last accessed: 7 November, 2013.

Gueymard, C. A.: Parameterized transmittance model for direct beam and circumsolar spectral irradiance, Sol. Energy, 71, 325–346, 2001.

Gueymard, C. A.: The sun's total and spectral irradiance for solar energy applications and solar radiation models, Sol. Energy, 76,

Table A1. AOD spectral scale factor ρ_{rj} for the rural aerosol mixture.

RH	Band 1	Band 2	Band 3	Band 4	Band 5	Band 6	Band 7	Band 8	Band 9	Band 10	Band 11	Band 12	Band 13	Band 14
0%	0.0738	0.1001	0.1286	0.1534	0.1887	0.2518	0.3017	0.4556	0.7163	1.0433	1.4023	1.7683	2.4499	0.0585
50%	0.0742	0.1006	0.1291	0.1540	0.1894	0.2525	0.3024	0.4563	0.7168	1.0433	1.4018	1.7673	2.4478	0.0588
70%	0.0755	0.1021	0.1308	0.1558	0.1914	0.2547	0.3047	0.4585	0.7183	1.0431	1.3995	1.7625	2.4372	0.0599
80%	0.0810	0.1087	0.1383	0.1640	0.2003	0.2644	0.3148	0.4682	0.7248	1.0415	1.3853	1.7326	2.3727	0.0647
90%	0.0826	0.1106	0.1405	0.1663	0.2028	0.2672	0.3177	0.4710	0.7266	1.0376	1.3614	1.6826	2.2664	0.0661
95%	0.0848	0.1131	0.1434	0.1694	0.2062	0.2709	0.3215	0.4746	0.7289	1.0348	1.3436	1.6459	2.1894	0.0680
98%	0.1085	0.1407	0.1741	0.2024	0.2415	0.3086	0.3602	0.5106	0.7522	1.0310	1.3054	1.5680	2.0289	0.0890
99%	0.1230	0.1571	0.1922	0.2215	0.2616	0.3298	0.3816	0.5300	0.7642	1.0275	1.2779	1.5128	1.9180	0.1020

Table A2. AOD spectral scale factor ρ_{rj} for the urban aerosol mixture.

RH	Band 1	Band 2	Band 3	Band 4	Band 5	Band 6	Band 7	Band 8	Band 9	Band 10	Band 11	Band 12	Band 13	Band 14
0%	0.1131	0.1460	0.1800	0.2086	0.2480	0.3155	0.3672	0.5170	0.7562	1.0389	1.3476	1.6541	2.2065	0.0932
50%	0.1123	0.1450	0.1789	0.2075	0.2469	0.3143	0.3659	0.5159	0.7555	1.0391	1.3494	1.6578	2.2141	0.0924
70%	0.1123	0.1450	0.1789	0.2075	0.2469	0.3143	0.3659	0.5159	0.7555	1.0399	1.3538	1.6669	2.2333	0.0924
80%	0.1022	0.1334	0.1661	0.1938	0.2324	0.2990	0.3504	0.5016	0.7465	1.0381	1.3503	1.6596	2.2179	0.0834
90%	0.1002	0.1311	0.1635	0.1911	0.2294	0.2959	0.3472	0.4987	0.7446	1.0344	1.3300	1.6180	2.1314	0.0816
95%	0.1043	0.1358	0.1687	0.1967	0.2354	0.3022	0.3536	0.5046	0.7484	1.0294	1.2990	1.5551	2.0027	0.0852
98%	0.1203	0.1541	0.1889	0.2181	0.2580	0.3260	0.3778	0.5266	0.7621	1.0220	1.2485	1.4548	1.8037	0.0996
99%	0.1397	0.1758	0.2124	0.2428	0.2838	0.3527	0.4046	0.5505	0.7767	1.0168	1.2108	1.3814	1.6629	0.1172

423–453, 2004.

Gueymard, C. A.: Prediction and validation of cloudless shortwave solar spectra incident on horizontal, tilted, or tracking surfaces, Sol. Energy, 82, 260–271, 2008.

Gueymard, C. A.: Temporal variability in direct and global irradiance at various time scales as affected by aerosols, Sol. Energy, 86, 3544–3553, 2012.

Gueymard, C. A. and Thevenard, D.: Monthly average clear-sky broadband irradiance database for worldwide solar heat gain and building cooling load calculations, Sol. Energy, 83, 1998–2018, 2009.

Holben, B., Eck, T., Slutsker, I., Tanre, D., Buis, J., Setzer, A., Vermote, E., Reagan, J., Kaufman, Y., Nakajima, T and, L. F., Jankowiak, I., and Smirnov, A.: AERONET: A federated instrument network and data archive for aerosol characterization, Rem. Sens. Environ., 66, 1–16, 1998.

Iacono, M. J., Delamere, J. S., Mlawer, E. J., Shephard, M. W., Clough, S. A., and Collins, W. D.: Radiative forcing by long-lived greenhouse gases: Calculations with the AER radiative transfer models, J. Geophys. Res. Atmos., 113, 2008.

Inman, R. H., Pedro, H. T., and Coimbra, C. F.: Solar forecasting methods for renewable energy integration, Prog. Energy Combust. Sci., 39, 535–576, 2013.

Iwabuchi, H.: Efficient Monte Carlo methods for radiative transfer modeling, J. Atmos. Sci., 63, 2324–2339, 2006.

Kinne, S., O'Donnel, D., Stier, P., Kloster, S., Zhang, K., Schmidt, H., Rast, S., Giorgetta, M., Eck, T. F., and Stevens, B.: MAC-v1: A new global aerosol climatology for climate studies, J. Adv. Mod. Earth Syst., 5, 704–740, 2013.

Lee, W.-L., Liou, K., and Hall, A.: Parameterization of solar fluxes over mountain surfaces for application to climate models, J. Geophys. Res. Atmos., 116, 2011.

Liou, K.: An introduction to atmospheric radiation, Vol. 84 of International Geophysics Series, Academic Press, San Diego, CA, Second Edn., 2002.

Long, C. N. and Ackerman, T. P.: Identification of clear skies from broadband pyranometer measurements and calculation of downwelling shortwave cloud effects, J. Geophys. Res., 105, 15 609–15, 2000.

MACC: http://www.gmes-atmosphere.eu/, Last accessed: 7 November, 2013.

Manners, J., Vosper, S., and Roberts, N.: Radiative transfer over resolved topographic features for high-resolution weather prediction, Q. J. R. Meteorol. Soc., 138, 720–733, 2012.

Mayer, B. and Kylling, A.: Technical note: The libRadtran software package for radiative transfer calculations - description and examples of use, Atmos. Chem. Phys., 5, 1855–1877, 2005.

Mayer, B., Hoch, S. W., and Whiteman, C. D.: Validating the MYSTIC three-dimensional radiative transfer model with observations from the complex topography of Arizona's Meteor Crater, Atmos. Chem. Phys., 10, 8685–8696, 2010.

Ohmura, A., Dutton, E. D., Forgan, B., Fröhlich, C., Gilgen, H., Hegner, H., Heimo, A., König-Langlo, G., McArthur, B., Müller, G., Philipona, R., Pinker, R., Whitlock, C. H., Dehne, K., and Wild, M.: Baseline Surface Radiation Network (BSRN/WCRP): New precision radiometry for climate research, Bull. Am. Meteorol. Soc., 79, 2115–2136, 1998.

Oreopoulos, L. and Barker, H. W.: Accounting for subgrid-scale cloud variability in a multi-layer 1d solar radiative transfer algorithm, Q. J. R. Meteorol. Soc., 125, 301–330, 1999.

Pincus, R. and Evans, K. F.: Computational cost and accuracy in calculating three-dimensional radiative transfer: Results for new implementations of Monte Carlo and SHDOM, J. Atmos. Sci., 66, 3131–3146, 2009.

Remer, L. A., Kaufman, Y., Tanré, D., Mattoo, S., Chu, D., Martins, J., Li, R.-R., Ichoku, C., Levy, R., Kleidman, R., Eck, T., Vermote, E., and Holben, B.: The MODIS aerosol algorithm, products, and validation, J. Atmos. Sci., 62, 947–973, 2005.

Table A3. Single-scattering albedo for the rural aerosol mixture.

RH	Band 1	Band 2	Band 3	Band 4	Band 5	Band 6	Band 7	Band 8	Band 9	Band 10	Band 11	Band 12	Band 13	Band 14
0%	0.8730	0.6695	0.8530	0.8601	0.8365	0.7949	0.8113	0.8810	0.9305	0.9436	0.9532	0.9395	0.8007	0.8634
50%	0.8428	0.6395	0.8571	0.8645	0.8408	0.8007	0.8167	0.8845	0.9326	0.9454	0.9545	0.9416	0.8070	0.8589
70%	0.8000	0.6025	0.8668	0.8740	0.8503	0.8140	0.8309	0.8943	0.9370	0.9489	0.9577	0.9451	0.8146	0.8548
80%	0.7298	0.5666	0.9030	0.9049	0.8863	0.8591	0.8701	0.9178	0.9524	0.9612	0.9677	0.9576	0.8476	0.8578
90%	0.7010	0.5606	0.9312	0.9288	0.9183	0.9031	0.9112	0.9439	0.9677	0.9733	0.9772	0.9699	0.8829	0.8590
95%	0.6933	0.5620	0.9465	0.9393	0.9346	0.9290	0.9332	0.9549	0.9738	0.9782	0.9813	0.9750	0.8980	0.8594
98%	0.6842	0.5843	0.9597	0.9488	0.9462	0.9470	0.9518	0.9679	0.9808	0.9839	0.9864	0.9794	0.9113	0.8648
99%	0.6786	0.5897	0.9658	0.9522	0.9530	0.9610	0.9651	0.9757	0.9852	0.9871	0.9883	0.9835	0.9236	0.8618

Table A4. Single-scattering albedo for the urban aerosol mixture.

RH	Band 1	Band 2	Band 3	Band 4	Band 5	Band 6	Band 7	Band 8	Band 9	Band 10	Band 11	Band 12	Band 13	Band 14
0%	0.4063	0.3663	0.4093	0.4205	0.4487	0.4912	0.5184	0.5743	0.6233	0.6392	0.6442	0.6408	0.6105	0.4094
50%	0.4113	0.3654	0.4215	0.4330	0.4604	0.5022	0.5293	0.5848	0.6336	0.6493	0.6542	0.6507	0.6205	0.4196
70%	0.4500	0.3781	0.4924	0.5050	0.5265	0.5713	0.6048	0.6274	0.6912	0.7714	0.7308	0.7027	0.6772	0.4820
80%	0.5075	0.4139	0.5994	0.6127	0.6350	0.6669	0.6888	0.7333	0.7704	0.7809	0.7821	0.7762	0.7454	0.5709
90%	0.5596	0.4570	0.7009	0.7118	0.7317	0.7583	0.7757	0.8093	0.8361	0.8422	0.8406	0.8337	0.8036	0.6525
95%	0.6008	0.4971	0.7845	0.7906	0.8075	0.8290	0.8418	0.8649	0.8824	0.8849	0.8815	0.8739	0.8455	0.7179
98%	0.6401	0.5407	0.8681	0.8664	0.8796	0.8968	0.9043	0.9159	0.9244	0.9234	0.9182	0.9105	0.8849	0.7796
99%	0.6567	0.5618	0.9073	0.9077	0.9182	0.9279	0.9325	0.9398	0.9440	0.9413	0.9355	0.9278	0.9039	0.8040

Ricchiazzi, P., Yang, S., Gautier, C., and Sowle, D.: SBDART: A research and teaching software tool for plane-parallel radiative transfer in the earth's atmosphere, Bull. Amer. Meteor. Soc., 79, 2101–2114, 1998.

Ritter, B. and Geleyn, J.-F.: A comprehensive radiation scheme for numerical weather prediction models with potential applications in climate simulations, Mon. Weather Rev., 120, 303–325, 1992.

Ruiz-Arias, J., Dudhia, J., Gueymard, C., and Pozo-Vázquez, D.: Assessment of the Level-3 MODIS daily aerosol optical depth in the context of surface solar radiation and numerical weather modeling, Atmos. Chem. Phys, 13, 675–692, 2013a.

Ruiz-Arias, J., Dudhia, J., Lara-Fanego, V., and Pozo-Vázquez, D.: A geostatistical approach for producing daily Level-3 MODIS aerosol optical depth analyses, Atmos. Environ., 79, 395–405, 2013b.

Ruiz-Arias, J. A., Cebecauer, T., Tovar-Pescador, J., and Šúri, M.: Spatial disaggregation of satellite-derived irradiance using a high-resolution digital elevation model, Sol. Energy, 84, 1644–1657, 2010.

Ruiz-Arias, J. A., Pozo-Váquez, D., Lara-Fanego, V., Santos-Alamillos, F. J., and Tovar-Pescador, J.: A high-resolution topographic correction method for clear-sky solar irradiance derived with a numerical weather prediction model, J. App. Meteorol. Clim., 50, 2460–2472, 2011.

Ruiz-Arias, J. A., Dudhia, J., Santos-Alamillos, F. J., and Pozo-Vázquez, D.: Surface clear-sky shortwave radiative closure intercomparisons in the Weather Research and Forecasting model, J. Geophys. Res. Atmos., 118, 9901–9913, 2013c.

Shettle, E. P. and Fenn, R. W.: Models for the aerosols of the lower atmosphere and the effects of humidity variations on their optical properties, Tech. Rep. AFGL-TR-79-0214, Air Force Geophys. Lab., 1979.

Short, K. C.: Spatial wildfire occurrence data for the United States, 1992-2011, Tech. Rep. FPA-FOD-20130422, USDA Forest Service, Rocky Mountain Research Station, Fort Collins, CO, doi:10.2737/RDS-2013-0009, 2013.

Zamora, R., Solomon, S., Dutton, E., Bao, J., Trainer, M., Portmann, R., White, A., Nelson, D., and McNider, R.: Comparing MM5 radiative fluxes with observations gathered during the 1995 and 1999 Nashville southern oxidants studies, J. Geophys. Res., 108, 4050, 2003.

Zamora, R. J., Dutton, E. G., Trainer, M., McKeen, S. A., Wilczak, J. M., and Hou, Y.-T.: The accuracy of solar irradiance calculations used in mesoscale numerical weather prediction, Mon. Weather Rev., 133, 783–792, 2005.

Table A5. Asymmetry parameter for the rural aerosol mixture.

RH	Band 1	Band 2	Band 3	Band 4	Band 5	Band 6	Band 7	Band 8	Band 9	Band 10	Band 11	Band 12	Band 13	Band 14
0%	0.7444	0.7711	0.7306	0.7103	0.6693	0.6267	0.6169	0.6207	0.6341	0.6497	0.6630	0.6748	0.7208	0.7419
50%	0.7444	0.7747	0.7314	0.7110	0.6711	0.6301	0.6210	0.6251	0.6392	0.6551	0.6680	0.6799	0.7244	0.7436
70%	0.7438	0.7845	0.7341	0.7137	0.6760	0.6381	0.6298	0.6350	0.6497	0.6657	0.6790	0.6896	0.7300	0.7477
80%	0.7336	0.7934	0.7425	0.7217	0.6925	0.6665	0.6616	0.6693	0.6857	0.7016	0.7139	0.7218	0.7495	0.7574
90%	0.7111	0.7865	0.7384	0.7198	0.6995	0.6864	0.6864	0.6987	0.7176	0.7326	0.7427	0.7489	0.7644	0.7547
95%	0.7009	0.7828	0.7366	0.7196	0.7034	0.6958	0.6979	0.7118	0.7310	0.7452	0.7542	0.7593	0.7692	0.7522
98%	0.7226	0.8127	0.7621	0.7434	0.7271	0.7231	0.7248	0.7351	0.7506	0.7622	0.7688	0.7719	0.7756	0.7706
99%	0.7296	0.8219	0.7651	0.7513	0.7404	0.7369	0.7386	0.7485	0.7626	0.7724	0.7771	0.7789	0.7790	0.7760

Table A6. Asymmetry parameter for the urban aerosol mixture.

RH	Band 1	Band 2	Band 3	Band 4	Band 5	Band 6	Band 7	Band 8	Band 9	Band 10	Band 11	Band 12	Band 13	Band 14
0%	0.7399	0.7372	0.7110	0.6916	0.6582	0.6230	0.6147	0.6214	0.6412	0.6655	0.6910	0.7124	0.7538	0.7395
50%	0.7400	0.7419	0.7146	0.6952	0.6626	0.6287	0.6209	0.6280	0.6481	0.6723	0.6974	0.7180	0.7575	0.7432
70%	0.7363	0.7614	0.7303	0.7100	0.6815	0.6550	0.6498	0.6590	0.6802	0.7032	0.7255	0.7430	0.7735	0.7580
80%	0.7180	0.7701	0.7358	0.7163	0.6952	0.6807	0.6801	0.6935	0.7160	0.7370	0.7553	0.7681	0.7862	0.7623
90%	0.7013	0.7733	0.7374	0.7203	0.7057	0.7006	0.7035	0.7192	0.7415	0.7596	0.7739	0.7827	0.7906	0.7596
95%	0.6922	0.7773	0.7404	0.7264	0.7170	0.7179	0.7228	0.7389	0.7595	0.7746	0.7851	0.7909	0.7918	0.7562
98%	0.6928	0.7875	0.7491	0.7393	0.7345	0.7397	0.7455	0.7602	0.7773	0.7883	0.7944	0.7970	0.7912	0.7555
99%	0.7021	0.7989	0.7590	0.7512	0.7613	0.7746	0.7718	0.7727	0.7867	0.7953	0.7988	0.7994	0.7906	0.7600

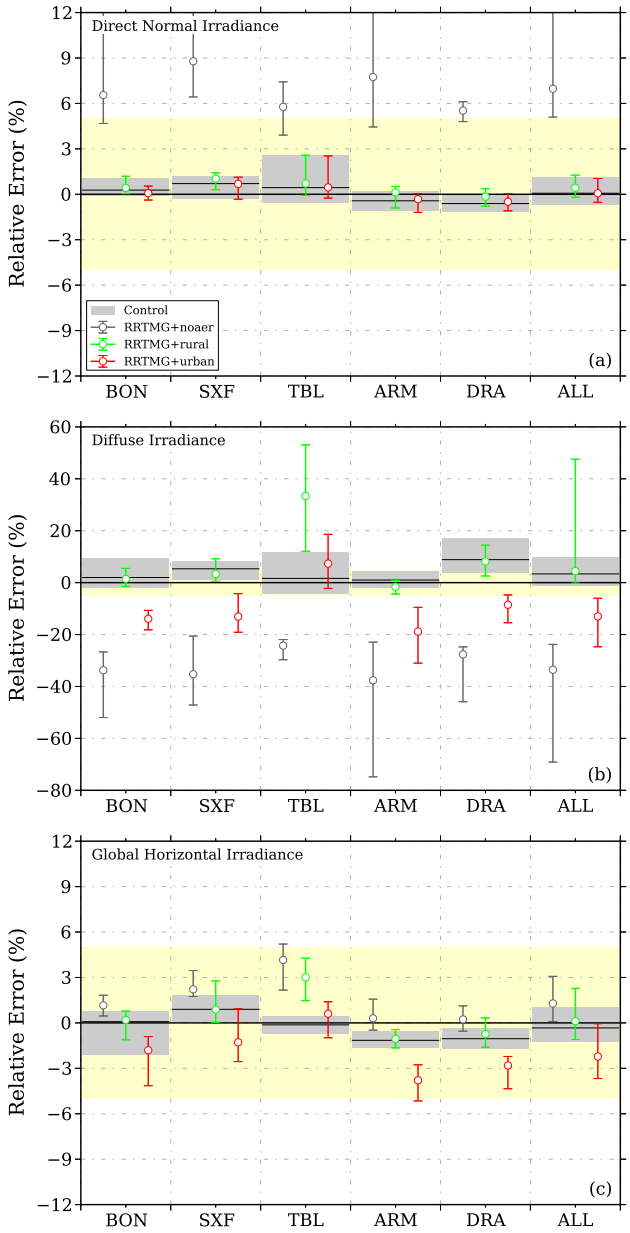

Fig. 3. Relative error of both the control experiment and the test cases as compared against the GHI, DNI and DIF ground observations at each site and the composite of all sites (ALL). The statistics are based on 767 samples for GHI and DIF and 892 for DNI. The number of samples per site varies between 150 and 200. The yellow-shaded area highlights the $\pm 5\%$ error region as a rough reference of the expected observational error. The grey blocks refer to the control experiment and encompass the region around the mean relative error (horizontal black line) that contains 66% of the experimental points at each site (33% above the mean error, and 33% below). The relative error obtained in the test cases is indicated with the vertical bars at each site. They also encompass 66% of the experimental points, the white circle mark being the mean relative error.

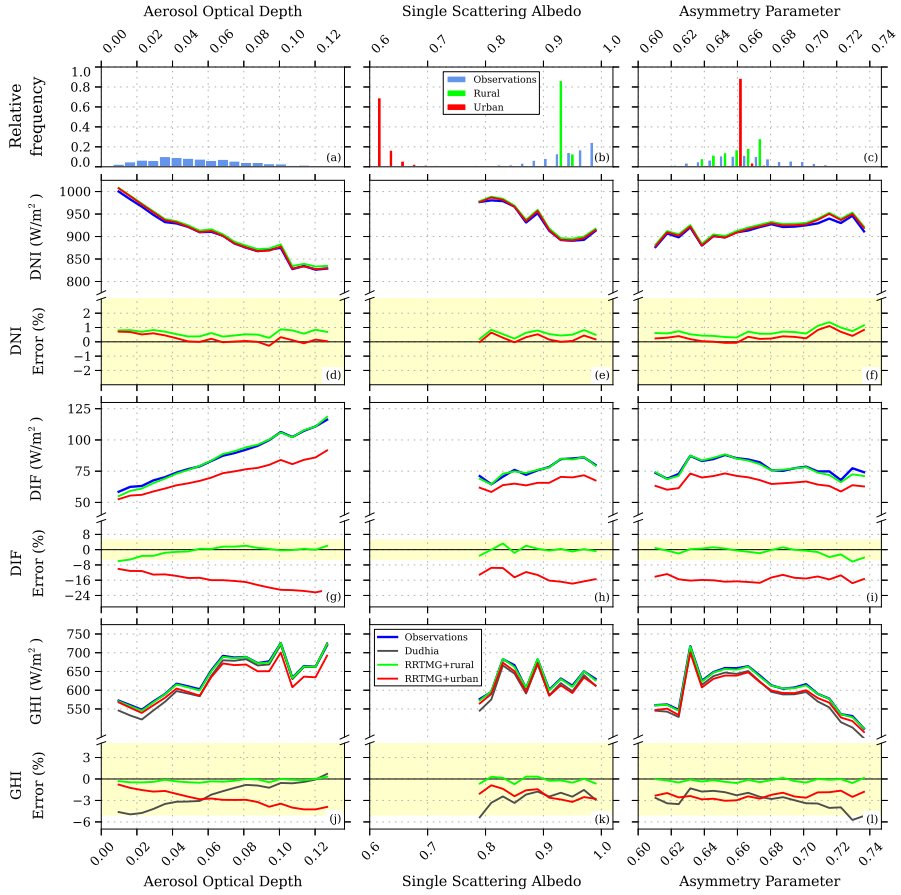

Fig. 4. Error analysis with respect to the variability range of AOD, SSA and ASY parameters for GHI, DNI and DIF resultant from the one-year WRF simulation. (a-c) shows the relative frequency distribution of the observed AOD at 0.55 µm, the observed and parameterized SSA values, and the observed and parameterized ASY values, respectively. (d-l) shows the observed and simulated DNI, DIF and GHI values (upper half of the panels) as well as their relative errors (lower half of the panels) as a function of the observed AOD at 0.55 µm, SSA and ASY values. The expected observational error region for the surface solar irradiance observations, roughly estimated as $\pm 5\%$, is highlighted in yellow.

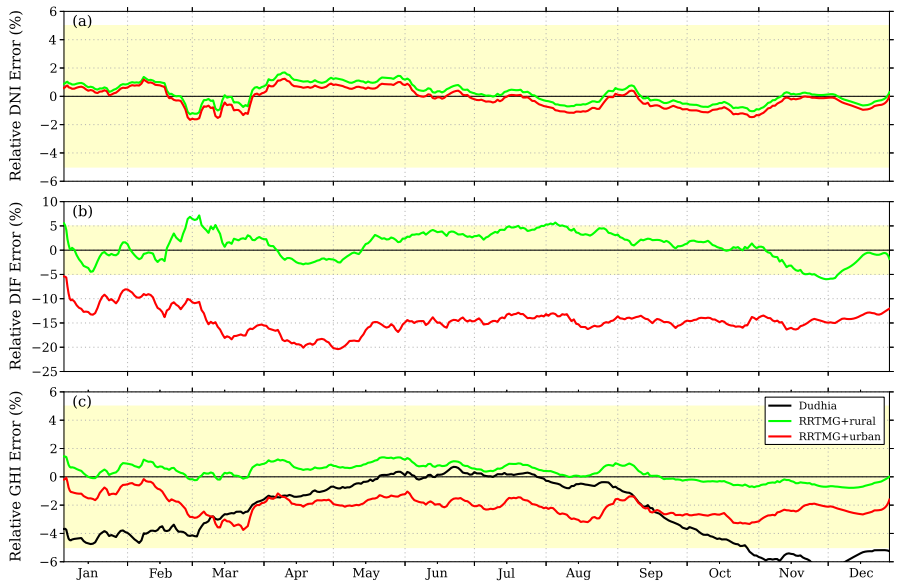

Fig. 5. Daily mean relative error in simulated DNI, DIF and GHI (simulated values minus observations, relative to the observations) using the RRTMG model assuming rural and urban aerosols, throughout the simulated year over the composite of the five experimental sites. A 15-day moving average filter has been used to make clear the bias trend. For GHI, the calculated values with the Dudhia scheme are also shown. The expected observational error region for the surface solar irradiance observations, roughly estimated as $\pm 5\%$, is highlighted in yellow.